NRC·CNRC

NRC Publications Archive
Archives des publications du CNRC

Modulating antibody-dependent cellular cytotoxicity of epidermal growth factor receptor-specific heavy-chain antibodies through hinge engineering

D'Eall, Calvin; Pon, Robert A.; Rossotti, Martin A.; Krahn, Natalie; Spearman, Maureen; Callaghan, Deborah; Van Faassen, Henk; Hussack, Greg; Stetefeld, Jörg; Butler, Michael; Durocher, Yves; Zhang, Jianbing; Henry, Kevin A.; Tanha, Jamshid

This publication could be one of several versions: author's original, accepted manuscript or the publisher's version. / La version de cette publication peut être l'une des suivantes : la version prépublication de l'auteur, la version acceptée du manuscrit ou la version de l'éditeur.
For the publisher's version, please access the DOI link below./ Pour consulter la version de l'éditeur, utilisez le lien DOI ci-dessous.

Publisher's version / Version de l'éditeur:
https://doi.org/10.1111/imcb.12238
Immunology and Cell Biology, 2019-01-29

NRC Publications Archive Record / Notice des Archives des publications du CNRC :
https://nrc-publications.canada.ca/eng/view/object/?id=b1c19e9c-0e81-4efb-bd78-4bc373cc5df3
https://publications-cnrc.canada.ca/fra/voir/objet/?id=b1c19e9c-0e81-4efb-bd78-4bc373cc5df3

Access and use of this website and the material on it are subject to the Terms and Conditions set forth at
https://nrc-publications.canada.ca/eng/copyright
READ THESE TERMS AND CONDITIONS CAREFULLY BEFORE USING THIS WEBSITE.

L'accès à ce site Web et l'utilisation de son contenu sont assujettis aux conditions présentées dans le site
https://publications-cnrc.canada.ca/fra/droits
LISEZ CES CONDITIONS ATTENTIVEMENT AVANT D'UTILISER CE SITE WEB.

Questions? Contact the NRC Publications Archive team at PublicationsArchive-ArchivesPublications@nrc-cnrc.gc.ca. If you wish to email the authors directly, please see the first page of the publication for their contact information.

Vous avez des questions? Nous pouvons vous aider. Pour communiquer directement avec un auteur, consultez la première page de la revue dans laquelle son article a été publié afin de trouver ses coordonnées. Si vous n'arrivez pas à les repérer, communiquez avec nous à PublicationsArchive-ArchivesPublications@nrc-cnrc.gc.ca.

National Research Council Canada | Conseil national de recherches Canada

Canada

Immunology & Cell Biology 2019; 1–12
www.wileyonlinelibrary.com/journal/icb

ORIGINAL ARTICLE

Modulating antibody-dependent cellular cytotoxicity of epidermal growth factor receptor-specific heavy-chain antibodies through hinge engineering

Calvin D'Eall[1,2,a], Robert A Pon[1,a], Martin A Rossotti[1], Natalie Krahn[3], Maureen Spearman[4], Deborah Callaghan[1], Henk van Faassen[1], Greg Hussack[1], Jörg Stetefeld[3], Michael Butler[4], Yves Durocher[5], Jianbing Zhang[1], Kevin A Henry[1] & Jamshid Tanha[1,2]

1 Human Health Therapeutics Research Centre, National Research Council Canada, 100 Sussex Drive, Ottawa, ON K1A 0R6, Canada
2 Department of Biochemistry, Microbiology and Immunology, University of Ottawa, 451 Smyth Road, Ottawa, ON K1H 8M5, Canada
3 Department of Chemistry, University of Manitoba, 144 Dysart Road, Winnipeg, MB R3T 2N2, Canada
4 Department of Microbiology, University of Manitoba, 144 Dysart Road, Winnipeg, MB R3T 2N2, Canada
5 Human Health Therapeutics Research Centre, National Research Council Canada, 6100 Royalmount Ave, Montréal, QC H4P 2R2, Canada

Keywords
antibody, antibody engineering, antibody-dependent cellular cytotoxicity (ADCC), epidermal growth factor receptor (EGFR), hinge, single-domain antibody

Correspondence
Jamshid Tanha, Human Health Therapeutics Research Centre, National Research Council Canada, 100 Sussex Drive, Ottawa, ON K1A 0R6, Canada.
E-mail: jamshid.tanha@nrc-cnrc.gc.ca

Present addresses
Natalie Krahn, Department of Molecular Biophysics and Biochemistry, Yale University, New Haven, CT, USA
Michael Butler, National Institute for Bioprocessing Research and Training, Dublin, Ireland
Jianbing Zhang, Xiangxue Pharma, Guangzhou, China

[a]Equal contributors.

Received 10 December 2018; Revised 22 January 2019; Accepted 22 January 2019

doi: 10.1111/imcb.12238

Immunology & Cell Biology 2019; 1–12

Abstract

Human IgG1 and IgG3 antibodies (Abs) can mediate Ab-dependent cellular cytotoxicity (ADCC), and engineering of the Ab Fc (point mutation; defucosylation) has been shown to affect ADCC by modulating affinity for FcRγIIIa. In the absence of a C_H1 domain, many camelid heavy-chain Abs (HCAbs) naturally bear very long and flexible hinge regions connecting their V_HH and C_H2 domains. To better understand the influence of hinge length and structure on HCAb ADCC, we produced a series of hinge-engineered epidermal growth factor receptor (EGFR)-specific chimeric camelid V_HH-human Fc Abs and characterized their affinities for recombinant EGFR and FcRγIIIa, their binding to EGFR-positive tumor cells, and their ability to elicit ADCC. In the case of one chimeric HCAb (EG2-hFc), we found that variants bearing longer hinges (IgG3 or camelid hinge regions) showed dramatically improved ADCC in comparison with a variant bearing the human IgG1 hinge, in similar fashion to a variant with reduced C_H2 fucosylation. Conversely, an EG2-hFc variant bearing a truncated human IgG1 upper hinge region failed to elicit ADCC. However, there was no consistent association between hinge length and ADCC for four similarly engineered chimeric HCAbs directed against distinct EGFR epitopes. These findings demonstrate that the ADCC of some HCAbs can be modulated simply by varying the length of the Ab hinge. Although this effect appears to be heavily epitope-dependent, this strategy may be useful to consider during the design of V_HH-based therapeutic Abs for cancer.

INTRODUCTION

The mechanisms of action of tumor-specific therapeutic antibodies (Abs) can be grouped into four general classes: (i) direct tumor cell killing, (ii) payload delivery, (iii) modification of the tumor microenvironment, and (iv) tumor cell killing by host immune cells.[1] Often, multiple modes of action contribute to the anti-tumor activity of a single Ab. Ab-dependent cellular cytotoxicity (ADCC) occurs when receptors on host effector cells [e.g. FcγRIIIa

and killer immunoglobulin-like receptors on natural killer (NK) cells] recognize Ab Fc regions in the context of infected or cancerous cells, leading to degranulation, cytokine secretion and tumor cell killing. ADCC occurs when the threshold of activation mediated through FcγRIIIa surpasses counterbalancing inhibitory signals, such as those mediated by killer immunoglobulin-like receptors. ADCC contributes to the clinical efficacy of therapeutic Abs against CD20,[2] epidermal growth factor receptor (EGFR),[3] HER2[4] and other targets.

Human IgG1 and IgG3 Abs are the major mediators of ADCC due to their low-affinity interaction with FcγRIIIa.[5] Historically, attempts to augment the ADCC of therapeutic Abs have focused on either increasing antigen-binding affinity through variable domain modification or enhancing FcγRIIIa binding through Fc modification (glycan or protein engineering). Through modification of a conserved *N*-linked biantennary oligosaccharide at C_H2 Asn297 (EU numbering), affinity and specificity for Fc receptors can be tailored to fit a desired therapeutic application;[6] for instance, C_H2 glycans lacking a core fucose moiety have been shown to augment ADCC responses by strengthening the Fc-FcγRIIIa interaction and amplifying NK cell activation.[7,8] Engineered Fc variants incorporating limited numbers of amino acid substitutions in their C_H2 and C_H3 domains have been designed to alter their interactions with Fc receptors and mediators of the complement system.[6]

Several studies have demonstrated that the effector functions of IgGs (ADCC and complement-dependent cytotoxicity; CDC) can be modulated by altering the length, flexibility and local conformation of their hinges. However, the consensus of these studies has been unclear. Truncation of the IgG3 hinge conferred either unchanged[9] or improved[10] ADCC and improved CDC,[11] although deletion of the IgG3 hinge region entirely abrogated ADCC with no effect on CDC.[12] Ablation of the disulfide linkage-forming Cys residues in the IgG1 hinge drastically impaired ADCC and slightly impaired CDC.[13] Decreasing the length or rigidity of the IgG1 middle hinge reduced ADCC and CDC,[14] while a His → Tyr substitution in the upper IgG1 hinge conferred elevated ADCC via increased affinity for FcγRIIIa.[15]

In addition to conventional Abs, camelid ruminants produce heavy-chain Abs (HCAbs) lacking C_H1 domains and light chains.[16] HCAbs consist of a single antigen-binding variable domain (V_HH) connected directly to the Fc by a hinge region that can vary in length from 12 to 35 residues. Recombinant HCAbs for therapeutic applications often bear human IgG1 hinge and Fc regions to enhance serum half-life and reduce the risk of immunogenicity. However, systematic studies exploring the ability of HCAbs to elicit effector functions such as ADCC, as well as the structural features of the hinge and Fc that influence their ADCC, are lacking. Here, we investigated the impact of hinge engineering on the ADCC of a panel of EGFR-directed HCAbs. We found that variants of one HCAb (EG2-hFc) bearing longer hinge regions (either a human IgG3 or camelid hinge) showed dramatically higher ADCC against EGFR-positive tumor cells compared with a variant bearing the human IgG1 hinge. However, this finding did not consistently extend to four other HCAbs directed against distinct EGFR epitopes. Overall, the data indicate that despite the naturally occurring long and flexible hinges of many camelid HCAbs, the structural parameters influencing the ADCC potential of chimeric HCAbs are probably similar to conventional Abs.

RESULTS

Biophysical characterization of chimeric HCAbs

We first produced a panel of chimeric HCAbs in which EG2, a previously described anti-EGFR V_HH,[17] was fused to human IgG1 Fc. Seven HCAb variants were produced (Figure 1 and Supplementary figure 1): (i) EG2-X1, consisting of EG2 fused to a human IgG1 hinge and Fc region; (ii) EG2-X2, a short-hinge variant bearing a seven-residue truncation in the upper IgG1 hinge region; (iii) EG2-X5, a variant bearing a human IgG1 hinge with a Cys → Ser substitution at position 220 (EU numbering); (iv) EG2-X6, a variant bearing the naturally occurring camelid 35-residue hinge; (v) EG2-X7, a variant bearing a human IgG1 hinge and a defucosylated C_H2 domain; (vi) EG2-X8, a variant bearing the 62-residue human IgG3 hinge; and (vii) EG2-X9, a variant in which the EG2 V_HH domain was fused to the C-terminus of Fc through a 25-residue $(Gly4Ser)_5$ linker. The chimeric HCAbs were expressed in either CHO-3E7 cells (EG2-X1, EG2-X2 and EG2-X7) or HEK293-6E cells (EG2-X1, EG2-X5, EG2-X6, EG2-X8 and EG2-X9). As a control, cetuximab was expressed in CHO-3E7 cells.

Following expression and purification, each chimeric HCAb variant showed bands on reducing and nonreducing SDS-PAGE corresponding to the expected molecular masses and was monodisperse by size exclusion chromatography (SEC), dynamic light scattering (DLS) and analytical ultracentrifugation (AUC) (Table 1 and Supplementary figure 2). The apparent molecular masses of the chimeric HCAbs, as estimated by SEC, deviated to various degrees from those calculated using the Svedberg equation from their experimentally determined hydrodynamic radii (r_H from DLS) and sedimentation coefficients ($s^0_{20,w}$ from AUC) as well as from their formula molecular masses. The short-hinge variant, EG2-X2, had the lowest apparent molecular mass, while the two long-hinge variants (EG2-X6 and EG2-X8, bearing camelid and

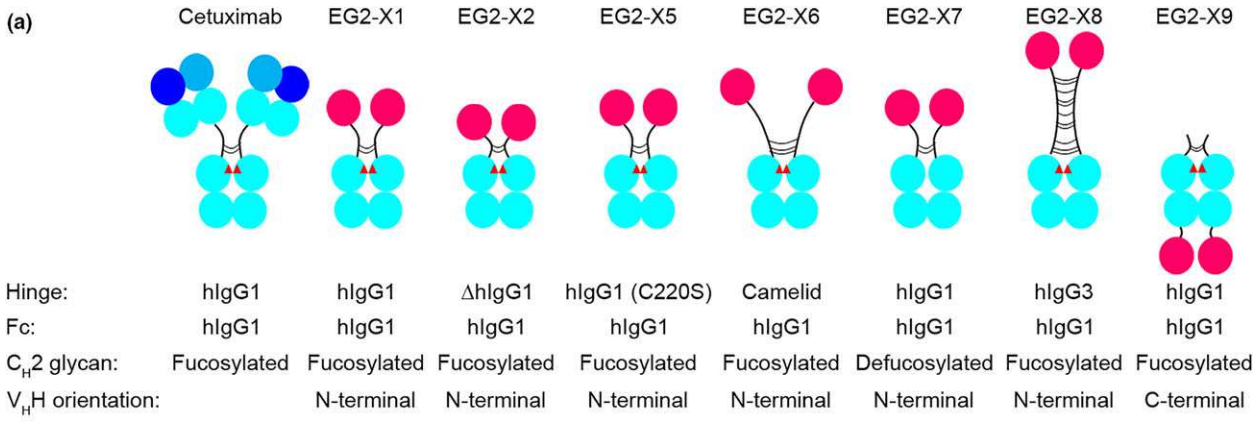

(b)

```
EG2-X1/7 ----------------------------------------------EPKSCDKTHTCPPCP
EG2-X2   ----------------------------------------------------THTCPPCP
EG2-X5   ----------------------------------------------EPKSSDKTHTCPPCP
EG2-X6   --------------------------EPKIPQPQPKPQPQPQPQPKPQPKPEPECTCPKCP
EG2-X8   ELKTPLGDTTHTCPRCPEPKSCDTPPPCPRCPEPKSCDTPPPCPRCPEPKSCDTPPPCPRCP
EG2-X9   ----------------------------------------------EPKSCDKTHTCPPCP
```

Figure 1. (a) Schematic structures, *N*-glycosylation and hinge modifications of cetuximab and the chimeric heavy-chain antibodies (HCAbs) used in this study. The core fucose moiety of the C_H2 Asn297 glycan is indicated by a triangle. The number of disulfide linkages in the human IgG1 and IgG3 hinges was assumed to be 2 and 11, respectively, and the maximum number of disulfide linkages (3) in the camelid hinge was assumed. **(b)** Hinge region sequences of chimeric HCAbs used in this study.

IgG3 hinges, respectively) as well as the C-terminally Gly4Ser-linked variant, EG2-X9, had disproportionately high apparent molecular masses (Table 1). These results demonstrated that structural changes in the hinge region with marginal impact on predicted molecular weight can have much larger effects on M_{SEC}, with long-hinge chimeric HCAbs (EG2-X6 and EG2-X8) having similar solvated molecular sizes as a full-length IgG (cetuximab).

The overall secondary structure elements of the chimeric HCAbs were similar, as shown by their circular dichroism spectra. All variants showed an ellipticity maximum at 200 nm and a minimum near 215 nm (Supplementary figure 2); EG2-X8 had a lower maximum at 200 nm, potentially due to the lower β-strand content of this chimeric HCAb. All variants showed monophasic unfolding as a function of temperature (presumably reflecting the similar T_ms of the V_HH, C_H2 and C_H3 domains), with T_ms ranging from 71.3 to 76.4°C (Table 1 and Supplementary figure 2).

Analysis of *N*-glycosylation

N-glycosylation analysis demonstrated that all of the chimeric HCAbs, as well as cetuximab, underwent predominantly complex-type glycosylation with minimal or no galactosylation (Figure 2a). No differences in glycosylation were observed between the two expression systems (CHO-3E7 and HEK293-6E). The dominant *N*-glycan observed for all variants except EG2-X7 was the fucosylated biantennary glycan, F(6)A2G0, with minor amounts of the more galactosylated species F(6)A2G1 and F(6)A2G2 detected. EG2-X7 was produced in CHO-3E7 cells treated with 5% (w/v) GDP-6-deoxy-D-lyxo-4-hexulose reductase, resulting in reduced fucosylation of the dominant biantennary *N*-glycan, A2G0. For this variant the dominant *N*-glycan was a nonfucosylated biantennary glycan, A2G0, with smaller amounts of the more galactosylated species A2G1 and A2G2 detected.

Binding to EGFR and FcRγIIIa

The monovalent binding affinities of the chimeric HCAbs to recombinant human EGFR were indistinguishable (Table 2 and Supplementary figure 3), albeit uniformly slightly weaker than previously reported affinity and kinetic parameters for EG2 V_HH.[17,18] Using mirrorball® microplate cytometry, all of the chimeric HCAbs bound to EGFR-positive MDA-MB-468 tumor cells (Figure 2b

Table 1. Biophysical characteristics of EG2-hFc variants.

	Cetuximab	EG2-X1	EG2-X2	EG2-X5	EG2-X6	EG2-X7	EG2-X8	EG2-X9
Expression cell line	CHO-3E7	CHO-3E7 and HEK293-6E	CHO-3E7	HEK293-6E	HEK293-6E	CHO-3E7	HEK293-6E	HEK293-6E
M_f (kDa)[a]	145.8	79.7	78.1	79.6	84.1	79.7	89.6	82.7
M_{SEC} (kDa)[b]	167	90	74	92	132	92	190	109
$M_{DLS,AUC}$[c]	162.7	85.8	82.8	84.5	84.2	84.5	99.0	94.0
$\bar{\upsilon}$ ($cm^3\ g^{-1}$)[d]	0.73	0.72	0.72	0.72	0.72	0.72	0.72	0.72
r_H (nm)[e]	5.62 ± 0.17	4.63 ± 0.16	4.16 ± 0.06	4.59 ± 0.12	4.87 ± 0.10	4.59 ± 0.04	5.71 ± 0.10	4.76 ± 0.04
$s^0_{20,w}$ (S)[f]	6.73 ± 0.04	4.36 ± 0.01	4.68 ± 0.06	4.33 ± 0.01	4.05 ± 0.09	4.33 ± 0.01	4.12 ± 0.08	4.71 ± 0.13
T_m (°C)[g]	71.3	74.3	71.6	73.1	74.3	74.6	75.2	76.4

AUC, analytical ultracentrifugation; DLS, dynamic light scattering; SEC, size exclusion chromatography.
[a]Theoretical MW calculated using the amino acid sequence and most prominent *N*-glycan.
[b]MW estimated by SEC using a Superdex 200 Increase 10/300 GL column.
[c]MW calculated from the Svedberg equation using experimentally determined r_H from DLS and $s^0_{20,w}$ from AUC.
[d]The partial specific volume ($\bar{\upsilon}$) was calculated using SEDNTERP.
[e]The hydrodynamic radius (r_H) was determined from DLS measurements at concentrations between 0.1 and 1.5 mg mL^{-1} extrapolated to infinite dilution.
[f]The Svedberg coefficient ($s^0_{20,w}$) was determined from AUC measurements at concentrations between 0.1 and 1.5 mg mL^{-1} extrapolated to infinite dilution and standard solvent conditions.
[g]Measured using circular dichroism.

and Table 2) but not to EGFR-low MCF7 cells (data not shown). Both long-hinge variants (EG2-X6 and EG2-X8) showed slightly lower EC_{50} and higher B_{max} values for binding to EGFR-positive cells while the C-terminally fused EG2-X9 variant showed very weak binding, potentially reflecting the formation of avid interactions by long-hinge variants or differences in exposure of the Fc to secondary reagents (especially for EG2-X9). We used microscale thermophoresis (MST) to determine the in-solution binding affinities of the chimeric HCAbs for FcγRIIIa. All of the HCAb variants and cetuximab showed virtually equivalent affinities for FcγRIIIa (K_D ~1–2 μM[19]), with the exception of the defucosylated variant, EG2-X7, which had ~10- to 20-fold higher affinity (K_D = 0.09 ± 0.02 μM) (Figure 2c and Table 2).

ADCC of chimeric HCAb variants

To assess the effect of hinge modification on the ADCC of the chimeric HCAbs, we purified NK cells from the peripheral blood of healthy donors and examined the ability of these cells to lyse ^{51}Cr-labeled EGFR-positive MDA-MB-468 tumor cells in the presence of each HCAb variant. An effector to target (E:T) cell ratio of 10:1 was used based on initial experiments with cetuximab showing that this ratio provided an optimal ADCC signal with minimal background of Ab-independent lysis (Supplementary figure 4). EG2-X1, bearing an unmodified human IgG1 hinge, had very weak ADCC that was not affected by the Cys220Ser substitution present in EG2-X5 (Figure 3a and Supplementary table 1). As expected, the defucosylated variant, EG2-X7, had markedly enhanced ADCC, paralleling similar effects reported for conventional Abs. Both the short-hinge HCAb variant EG2-X2 and the C-terminally fused variant EG2-X9 failed to elicit ADCC. By contrast, HCAb variants bearing the longer camelid or human IgG3 hinge regions (EG2-X6 and EG2-X8) displayed dramatically increased ADCC, with EC_{50} potencies 2–3-log-fold lower than EG2-X1. These trends were consistent across 4–6 independent experiments using NK cells derived from different donors (Supplementary figure 5). No effects of either donor FcγRIIIa allotype or expression cell line (CHO-3E7 *versus* HEK293-6E) on ADCC were observed (Supplementary figure 6 and Supplementary table 2).

To assess whether the effects of HCAb hinge length modification on ADCC were general, we used an ADCC reporter assay in which luciferase expression is driven by an NFAT response element in stably transfected FcRγIIIa-expressing Jurkat cells.[20] We examined the effect of replacing the human IgG1 hinge with longer camelid or human IgG3 hinges in V_HHs directed against four other distinct EGFR epitopes.[18] These V_HHs all had

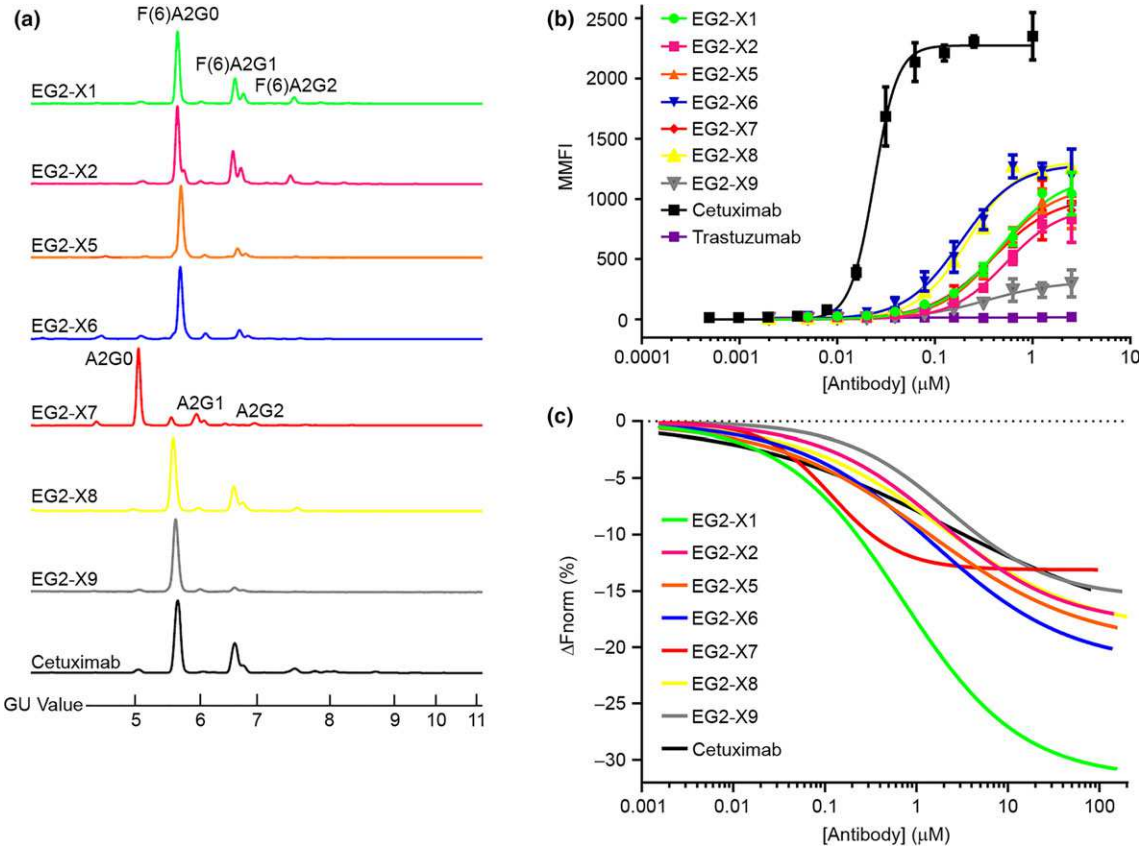

Figure 2. *N*-glycosylation, epidermal growth factor receptor (EGFR)-positive cell-binding and FcγRIIIa binding of antibodies used in this study. **(a)** *N*-glycan analysis of cetuximab and EG2 chimeric heavy-chain antibodies (HCAbs). Glucose unit (GU) values were calculated for the eluted peaks based on the dextran ladder profile. Results represent a single experiment. **(b)** Binding of cetuximab and EG2-hFc variants to EGFR-positive MDA-MB-468 cells by mirrorball® microplate cytometry. Data are presented as means ± s.e.m. of triplicate measurements from individual experiments. Cell binding EC_{50} values are presented in Table 2. MMFI, median mean fluorescence intensity. Results are representative of three independent experiments, each with three replicates. **(c)** Binding of cetuximab and EG2 chimeric HCAbs to FcγRIIIa (158F) by microscale thermophoresis. Each data point correlates to the normalized fluorescence (± s.d.) of a single standard glass capillary containing fluorescently labeled FcγRIIIa and unlabeled Abs at a specified concentration. Affinity constants (K_Ds) were determined by fitting the binding curve using a quadratic solution to the law of mass action for the fraction of fluorescent molecules that formed a complex and are presented in Table 2. EG2-X1 was assayed with a different preparation of fluorescenated FcγRIIIa than the other variants with higher labeling efficiency, resulting in a larger maximal fluorescence change. Results are representative of three independent experiments, each with two replicates.

monovalent affinities for recombinant EGFR in the same range as EG2 and cetuximab (1–10 nM) and bound well to EGFR-positive tumor cells.[18] The reporter assay showed similar trends in terms of the increased ADCC of long-hinge variants of EG2 shown in the ^{51}Cr-release assay (Figure 3b and Supplementary table 1). However, for the other four V_HHs tested, replacement of the human IgG1 hinge with camelid or human IgG3 hinges either had no effect on or impaired ADCC (Figure 3c–f and Supplementary table 1). The only potential exception was NRC-sdAb028: a variant of this HCAb bearing an IgG3 hinge showed moderately improved ADCC compared with variants bearing either a human IgG1 or camelid hinge. No consistent association between ADCC and the hinge length of chimeric HCAbs was observed, as in all four cases variants bearing human IgG3 and camelid hinges showed widely different ADCC. Variation in the ADCC of chimeric HCAbs was not due to differences in binding to EGFR-positive tumor cells, which was similar for the X1, X8 and X9 variants of each chimeric HCAb (Supplementary figure 7).

DISCUSSION

Numerous studies have examined the effects of Fc and hinge modification on the ADCC and CDC of full-length

Table 2. Binding of EG2-hFc variants to EGFR and FcγRIIIa.

	Cetuximab	EG2-X1	EG2-X2	EG2-X5	EG2-X6	EG2-X7	EG2-X8	EG2-X9
EGFR K_D (nM)[a]	0.7	81.6	124	82.7	81.3	111	84.0	80.7
EGFR$^+$ cell EC_{50} (nM)[b]	23.7 ± 0.7	467 ± 68	532 ± 65	433 ± 53	183 ± 18	390 ± 58	217 ± 22	n.b.[d]
FcγRIIIa K_D (μM)[c]	1.0 ± 0.4	0.8 ± 0.2	2.0 ± 0.5	1.5 ± 0.5	1.1 ± 0.4	0.09 ± 0.02	2.0 ± 1.5	1.5 ± 0.5

EGFR, epidermal growth factor receptor; MST, microscale thermophoresis; SPR, surface plasmon resonance.
[a]Determined via SPR by Fc-capturing the variant and flowing human EGFR over the resulting surface.
[b]Determined by mirrorball® microplate cytometry.
[c]Determined from the MST binding curve using a quadratic solution to the law of mass action.
[d]Nonsigmoidal binding from which EC_{50} could not be determined.

IgGs. For example, substitutions of specific C_H2/C_H3 residues,[6] reduced C_H2 fucosylation,[7,8] and a single-site substitution in the upper IgG1 hinge (His → Tyr)[15] resulted in enhanced ADCC via increased affinity for FcγRIIIa. Previous work also suggested a complex role of hinge length, composition and flexibility on the ADCC of IgGs.[9-15] However, systematic studies exploring the ability of HCAbs to elicit ADCC, as well as the structural features of the hinge and Fc regions of chimeric HCAbs that influence ADCC, are lacking. These features might be expected to differ from those of full-length IgGs, given the proximity of Fc to the V_HH domain in complex with antigen.

Here, we attempted to address these unknowns by assessing the ADCC of a series of hinge- and glyco-engineered chimeric HCAbs. We based the majority of our analyses on chimeric HCAb variants of EG2, a V_HH that has previously been reported to bind human EGFR with a monovalent K_D of 15–55 nM.[17,18] In the current study, all chimeric HCAbs bearing EG2 showed weaker monovalent K_Ds for EGFR between 80 and 120 nM, primarily due to a slower on-rate compared with previous studies (Supplementary figure 3). This discrepancy may have arisen from differences in the surface plasmon resonance assay orientation (capture Ab, flow antigen) compared with previous work, or potentially from low activity of the recombinant EGFR used in this study. Regardless, we found no evidence that modulation of the hinge region of these chimeric HCAbs affected the intrinsic EGFR-binding affinity of EG2 V_HH. However, as reported previously,[18] binding of EG2 chimeric HCAbs (regardless of hinge sequence) to EGFR-positive MDA-MB-468 cells was much weaker than expected based on its monovalent affinity for recombinant EGFR, probably reflecting limited accessibility of this epitope on native cell-surface EGFR.

Both EG2-X6 and EG2-X8 chimeric HCAbs showed slightly lower EC_{50} and higher B_{max} values for binding to EGFR-positive cells than other variants (Figure 2b). While it is possible that the minor changes in these binding parameters (~2- or 3-fold) may be connected with the drastically improved ADCC of these variants, we note that (i) several chimeric HCAbs, for which no differences in binding were observed regardless of hinge sequence, showed drastically reduced ADCC (Figure 3c–f), and (ii) chimeric HCAbs incorporating the NRC-sdAb032 V_HH showed significantly lower EC_{50}s for binding to EGFR-positive cells than other variants without a commensurate increase in ADCC. Thus, we caution against any simplistic interpretation involving a consistent and direct association between binding and ADCC potency. Conceivably, however, the improved binding of EG2-X6 and EG2-X8 to EGFR-positive cells might reflect avid interaction with two receptors, which could dramatically potentiate ADCC via improved residence time or promoting Fc conformational changes favorable for immune synapse formation.

We carried out extensive biophysical characterization of this panel of chimeric HCAbs. All of the HCAb variants were monodisperse, aggregate-free and equivalently thermostable. With the exception of the defucosylated HCAb, EG2-X7, all of the chimeric HCAbs showed Fc glycosylation patterns similar to cetuximab[21] regardless of the expression system used. The only notable difference among the EG2 chimeric HCAbs was in their apparent molecular masses as determined by SEC and AUC/DLS: in comparison with the variant bearing a human IgG1 hinge (EG2-X1), both long-hinge variants (EG2-X6 and EG2-X8) as well as the C-terminally fused variant (EG2-X9) had larger solvated molecular sizes while the variant bearing a truncated human IgG1 hinge (EG2-X2) had a smaller solvated molecular size. By contrast, AUC and DLS analyses calculated appropriate molecular weights for all variants. Thus, we were confident that any differences in ADCC among the chimeric HCAbs did not result from either large-scale variation in EGFR-binding affinity or from biophysical or glycosylation changes (with the exception of the defucosylated EG2-X7 variant).

The ADCC of all of the EG2 chimeric HCAb variants were dramatically less potent than that of cetuximab, presumably owing to cetuximab's superior intrinsic

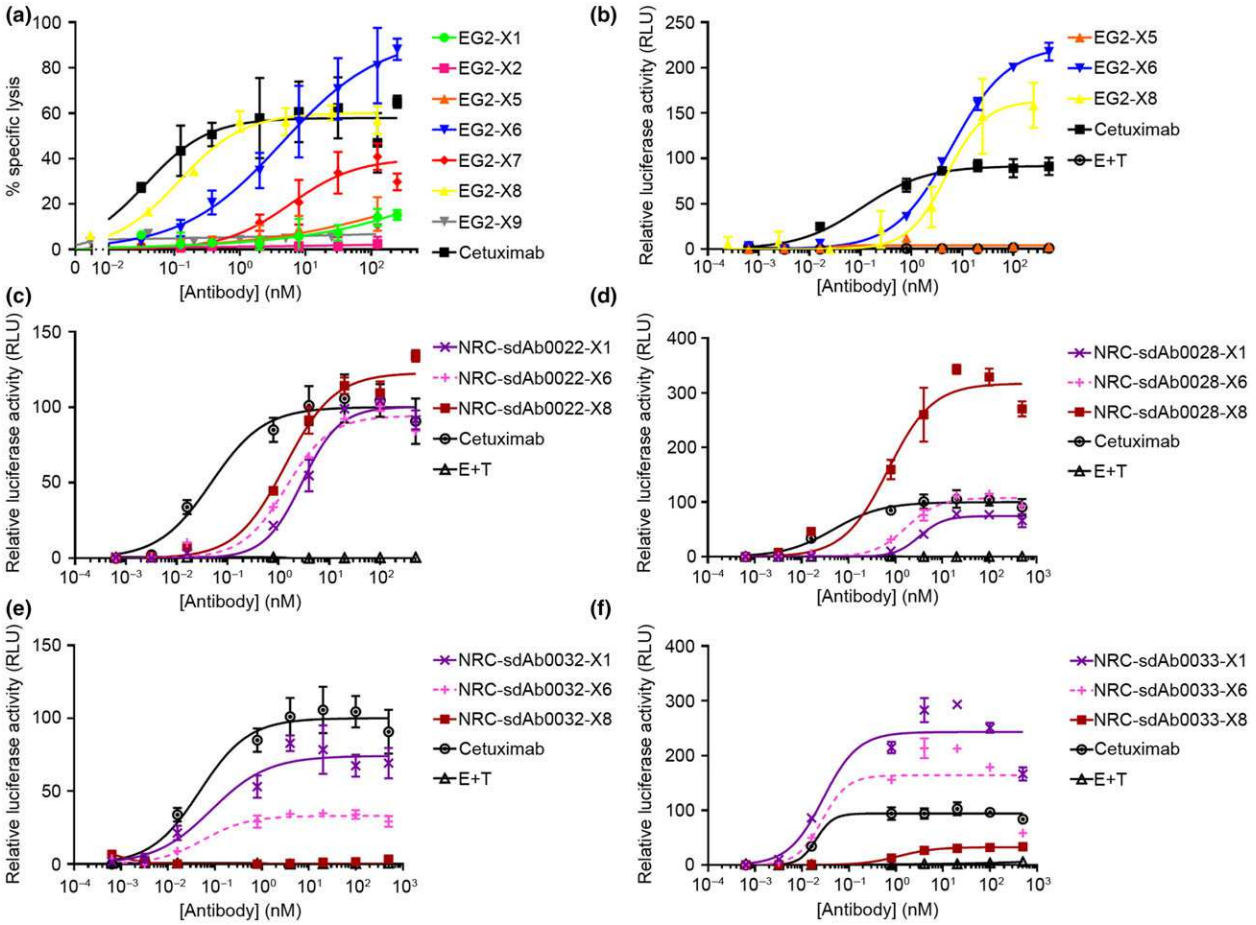

Figure 3. Influence of hinge length and composition on antibody-dependent cellular cytotoxicity (ADCC) of chimeric heavy-chain antibodies (HCAbs). **(a)** ADCC of chimeric EG2 HCAbs measured using a ^{51}Cr-release assay. The data shown are representative of 2–5 experiments for each variant, with each experiment conducted in triplicate using primary natural killer effector cells derived from a single donor (Supplementary figure 5). **(b)** ADCC of selected chimeric EG2 HCAbs measured using a reporter bioassay. The increased ADCC of long-hinge EG2 variants was consistent across both assays. **(c–f)** The ADCC of chimeric HCAbs comprising four additional V_HHs directed against distinct EGFR epitopes (NRC-sdAb022, NRC-sdAb028, NRC-sdAb032 and NRC-sdAb033) and either a human IgG1, human IgG3 or camelid hinge was measured using a reporter bioassay. In panels **(b–f)**, the data shown are of a single experiment comprising three replicates, and are representative of at least three independent experiments.

affinity for EGFR and, potentially, better accessibility of its epitope on cells, leading to denser accumulation of the Ab on the cell surface. We confirmed that as in IgGs, defucosylation of the C_H2 domains of chimeric HCAbs (EG2-X7) resulted in increased ADCC due to improved binding to FcγRIIIa, despite the closer proximity of C_H2 to the cell surface in these molecules. The EG2-X1 variant bearing a human IgG1 hinge had only marginal ADCC and replacement of the vestigial upper-hinge Cys (which in IgG1s forms a disulfide linkage with the C_L domain) with Ser in the EG2-X5 variant did not alter ADCC. Despite apparently similar binding to EGFR-positive tumor cells (Figure 2b) and FcγRIIIa (Figure 2c), the short-hinge variant bearing a truncated upper IgG1 hinge (EG2-X2) elicited low or no ADCC compared with EG2-X1, although the magnitude of this change was difficult to estimate given the very weak activity of both molecules. This result was in agreement with an earlier study of ADCC-deficient IgG1s bearing truncated middle hinges,[14] and reflects the site of the Fc-FcγRIIIa interaction at the lower hinge-C_H2 junction; the authors suggested that hinge shortening resulted in steric occlusion of FcγRIIIa by the Fab arms. The IgG3 hinge may have more tolerance to truncation due to its longer length.[9,10] Alternatively, IgGs and chimeric HCAbs with truncated IgG1 hinges may lack sufficient segmental

flexibility to achieve the asymmetrical configuration of the Fab/V_HH arms around the central Fc required for exposure of the FcγRIIIa binding site.[22]

Based on the reduced ADCC of chimeric HCAbs with truncated IgG1 hinges, we explored the potential of hinge extension to potentiate ADCC. Both chimeric HCAbs bearing a 35-residue camelid hinge (EG2-X6) and a human IgG3 hinge (EG2-X8) exhibited dramatically improved ADCC. This difference was not easily explainable by changes in binding to either recombinant EGFR or EGFR-positive tumors, nor to changes in FcγRIIIa binding. Thus, we assume that the increased ADCC of these variants resulted from a combination of (i) improved avidity for cell-surface EGFR, although this was only modestly detectable in cytometry assays (Figure 2b), (ii) increased exposure/availability of Fc on target cells for engagement by native FcγRIIIa on NK cells, although this was not reflected in *in vitro* binding assays using recombinant FcγRIIIa (Figure 2c), and/or (iii) altered geometry and/or increased flexibility of long-hinge HCAbs, allowing for more efficient formation of NK cell:target cell immunological synpases. Together these factors contributed to optimal immune synapse formation between NK cells and tumor cells coated with chimeric EG2-X6 and EG2-X8 HCAbs. However, for four other chimeric HCAbs directed against distinct EGFR epitopes, hinge extension had apparently unreliable effects on ADCC and often compromised it severely, and thus we conclude that this effect is strongly epitope-dependent for HCAbs and presumably for full-length IgGs as well. In agreement with this notion, ADCC, CDC and Ab-dependent phagocytosis were found to depend heavily on epitope distance from the cell membrane in several model systems, albeit possibly in an antigen-specific manner.[23,24] Moreover, ADCC clearly depends not only on hinge length but its sequence, geometry and conformation, as shown by the widely differing ADCC of chimeric HCAbs bearing human IgG3 and camelid hinges (both longer than human IgG1 hinge). In a C-terminal fusion orientation (EG2-X9), however, an extended 25-residue flexible Gly-Ser linker conferred increased solvated molecular size but decreased binding to EGFR-positive tumor cells and abrogation of ADCC this might reflect the inability of the EG2 V_HH to access its EGFR epitope on the surface of tumor cells in this orientation and/or, for the cell-bound chimeric HCAb, inaccessibility of Fc for binding by anti-Fc Abs or NK cell-surface FcγRIIIa.

In conclusion, we have shown that (i) defucosylation of chimeric HCAb C_H2 domains enhances ADCC through increased affinity for FcγRIIIa, and that (ii) increasing the hinge length of some chimeric HCAbs can significantly enhance or decrease ADCC, although this effect appears to be strongly epitope-dependent. We did not examine the effects of combining hinge engineering with other Fc modifications (C_H2 defucosylation, site-specific mutations) on ADCC, although this strategy could be addressed in future studies. Structural information and modeling studies may shed insight into the mechanism underlying the increased ADCC of chimeric EG2 HCAbs with extended hinges, and may also suggest whether the success of this strategy can be predicted *a priori*. Future studies could also examine whether similar effects on ADCC can be achieved by hinge engineering of conventional IgGs as well as whether CDC can be modulated using similar strategies. Given the ability of HCAbs to interact with recessed epitopes such as enzyme active sites,[25] it is possible that a subset of naturally occurring camelid HCAb IgGs evolved very long and flexible hinges to potentiate the effector function of molecules whose binding arms are closely spaced and, in the absence of a C_H1 domain, lie in close proximity to the Fc.[26]

METHODS

Primary cells and cell lines

Fresh whole blood (500 mL) was obtained with informed consent from healthy donors following institutional ethics approval (netCAD; Canadian Blood Services, Vancouver, BC, Canada). Buffy layers were prepared from whole blood diluted 1:1 with 0.9% saline and centrifuged at 300 $\times g$ for 30 min. After further dilution (1:1) with Dulbecco's phosphate-buffered saline (PBS; Sigma-Aldrich, St Louis, MO, USA), peripheral blood mononuclear cells (PBMCs) were isolated by density gradient centrifugation over Ficoll-Paque PLUS (GE Healthcare, Piscataway, NJ, USA) at 300 $\times g$ for 30 min. PBMCs were washed twice with PBS, resuspended in RPMI-1640 medium supplemented with 10% (v/v) heat-inactivated fetal bovine serum, 2 mM L-glutamine, 100 μg mL^{-1} penicillin and 100 μg mL^{-1} streptomycin (all from Sigma-Aldrich), and then stimulated overnight (1×10^8 cells per T75 flask, 37°C, 5% CO_2) with 50 U mL^{-1} of recombinant human interleukin-2 (IL-2; Novartis, Emeryville, CA, USA). IL-2 stimulation was strictly limited to ≤15 h duration.

The EGFR-positive and EGFR-low human breast adenocarcinoma cell lines MDA-MB-468 and MCF-7 (ATCC, Manassas, VA, USA) were cultured at 37°C in RPMI-1640 media supplemented as described above under an atmosphere containing 5% CO_2 and 90% humidity. Both cell lines were trypsinized and subcultured weekly up to a maximum of 10 passages. Cells used in binding assays were between 70% and 80% confluent.

Antibody expression and purification

Cetuximab and three chimeric HCAbs (EG2-X1, EG2-X2 and EG2-X7) were expressed in CHO-3E7 cells as previously described.[27] For expression of EG2-X7, CHO-3E7 cells were

supplemented with 5% GDP-6-deoxy-D-lyxo-4-hexulose reductase to reduce core fucosylation of the C_H2 Asn297 glycan.

All other chimeric HCAbs were expressed in HEK293-6E cells. Briefly, HEK293-6E cells were cultured in Gibco® FreeStyle F17 expression medium (Thermo Fisher Scientific, Waltham, MA, USA) supplemented with 4 mM L-glutamine, 0.1% (w/v) pluronic acid and 50 μg mL^{-1} geneticin (Thermo Fisher) at 37°C under an atmosphere containing 5% CO_2 and 60% humidity, 5% CO_2 with 100 rpm shaking. When a density of 1.5–2 × 10^6 cells mL^{-1} was achieved, cells were transfected using PEIpro (Polyplus-transfection® SA, Illkirch, France). DNA and PEIpro were mixed 1:1 (100 μg each), vortexed three times and incubated for 3 min at room temperature before adding to cells. Five days later, cell suspensions were centrifuged at 300 ×*g* for 10 min and the supernatants were passed through 0.2-μm filters (EMD Millipore, Burlington, MA, USA) and gravity-fed over MabSelect SuRe protein A affinity columns according to the manufacturer's instructions (GE Healthcare). The chimeric HCAbs were eluted using 100 mM sodium citrate, pH 3.6, immediately neutralized using 1 M Tris, pH 8.8, and then dialyzed overnight against PBS. Ab concentrations were determined using absorbance at 280 nm. Protein purity was assessed by reducing and nonreducing SDS-PAGE.

Size exclusion chromatography

Purified Abs (1 mg mL^{-1}) in PBS were injected over a Superdex 200 Increase 10/300 GL column (GE Healthcare) connected to an ÄKTA FPLC protein purification system (GE Healthcare) at a flow rate of 0.8 mL min^{-1}. To estimate each Ab's molecular mass, a standard curve (log M_f *versus* elution volume) was generated for a set of gel filtration standards (Cat. No. 1511901; Bio-Rad, Hercules, CA, USA) and then the apparent molecular mass (M_{SEC}) of each Ab was calculated by interpolation.

N-glycosylation analysis

Ab *N*-glycans were released by binding to a protein A column and PNGase F digestion following a previously described protocol[28] and analyzed by hydrophobic interaction liquid chromatography[21] at a flow rate of 0.86 mL min^{-1} using an X-Bridge 3.5-μm amide column (4.6 × 250 mm; Waters, Milford, MA, USA) heated to 30°C with fluorescent detection. *N*-glycans were eluted using a 50 mM ammonium formate, pH 4.4: acetonitrile gradient (1:4 increasing to 1:1 ratio over 48 min). Peaks were calibrated using a 2-amino benzamide-labeled glucose ladder and glycan standards[29] (Prozyme, Hayward, CA, USA) before comparing to a glycan database (www.glycobase.nibrt.ie) for preliminary identification. Structures were confirmed as described previously using exoglycosidase digestion.[21]

Circular dichroism

Far-UV circular dichroism spectra were recorded on a J-810 spectropolarimeter (Jasco Inc., Easton, PA, USA) calibrated using 2.6 mM (1S)-(+)-camphor-10-sulfonic acid monohydrate (Alfa Aesar, Ward Hill, MA, USA). Measurements were taken from 190 to 250 nm using a 1.0 mm quartz cuvette and an integration time of 8 s nm^{-1}. Ab samples were prepared at a concentration of 1.5 μM in 10 mM sodium phosphate, pH 7.5, containing 154 mM NaF. Samples and buffer were measured in triplicate, corrected with the calibration factor, averaged and baseline-subtracted. All spectra were normalized by the number of peptide bonds per unit volume.

Ab melting temperatures were determined using a Jasco J-815 spectropolarimeter (Jasco Inc.) in 100 mM sodium phosphate, pH 7.4, according to a previously described method[30] with minor modifications. Briefly, Ab solutions (50 μg mL^{-1}) were placed in 5-mm quartz cuvettes and thermal unfolding was followed at 202 nm with ellipticity measurements taken every 0.2°C from 25 to 96°C with a temperature ramp rate of 1°C min^{-1}. The folded protein fraction was calculated from molar ellipticity and then plotted against temperature and fitted to a Boltzmann sigmoidal distribution in Graphpad Prism 6 to determine the thermal unfolding midpoint (T_m).

Hydrodynamic studies

DLS studies of Abs were performed as previously described[31-33] at Ab concentrations ranging from 0.1 to 1.5 mg mL^{-1}. Ab homogeneity was studied by AUC using a sedimentation velocity method in a ProteomeLab XL-I instrument fitted with an An50 Ti 8-cell analytical rotor (Beckman Coulter Inc., Brea, CA, USA). Standard 12-mm double-sector cells were filled with 400 μL of Ab in the sample channel and 420 μL of 10 mM sodium phosphate, pH 7.5, containing 154 mM NaF in the buffer channel. A total of 90 absorbance and interference radial scans were collected at 20°C every 11.5 min at a speed of 72 500 ×*g*. Data analysis was performed using the SEDFIT program[34,35] to determine the sedimentation coefficients of each Ab ($s_{20,b}$). The sedimentation coefficients were then converted to standard solvent conditions ($s_{20,w}$) using the buffer viscosity and density calculated from SEDNTERP[36] and finally extrapolated to infinite dilution ($s^0_{20,w}$).

Surface plasmon resonance

Monovalent binding between EG2 hinge variants and recombinant human EGFR ectodomain was studied by single-cycle kinetic analysis using a Biacore T200 instrument (GE Healthcare) at 25°C in PBS containing 0.05% (v/v) surfactant P20. Recombinant human EGFR ectodomain (Cat. No. Z03194; Genscript, Piscataway, NJ, USA) was purified by preparative SEC using a Superdex 200 Increase 10/300 GL column (GE Healthcare) connected to an ÄKTA FPLC protein purification system prior to surface plasmon resonance analyses. Briefly, approximately 5000 response units of goat anti-human IgG (Jackson ImmunoResearch, West Grove, PA, USA) were immobilized on a Series S sensor chip CM5 (GE Healthcare) by amine coupling in 10 mM actetate buffer, pH 4.5. EG2 hinge variants or cetuximab (2.5 μg mL^{-1}) were captured at a flow rate of 10 μL min^{-1}, then EGFR (five concentrations ranging from 0.3 to 50 nM) was injected over

the resulting surfaces at a flow rate of 30 μL min^{-1} with a 180 s contact time and a 600 s dissociation phase. The surfaces were regenerated with a 10 s pulse of 10 mM glycine, pH 1.5. Data were analyzed using Biacore T200 software version 3.0 (GE Healthcare) and fit to a 1:1 binding model.

Mirrorball® microplate cytometry

Binding to EGFR-positive and EGFR-low tumor cell lines was assessed using a mirrorball® high-sensitivity microplate cytometer (TTP Labtech Inc, Melbourn, UK). EGFR-positive MDA-MB-468 cells and EGFR-low MCF-7 cells were dissociated in Accutase® solution (Sigma-Aldrich), washed with Hank's Balanced Salt Solution (Thermo Fisher) and counted. Cells (4000 cells $well^{-1}$) were seeded in Nunc® MicroWell 96-well optical bottom plates (Sigma-Aldrich) and incubated at 37°C in a humidified atmosphere containing 5% CO_2 for 24–48 h. Each Ab was serially diluted in Live Cell Imaging Solution (LCIS; Thermo Fisher) and 50 μL of each Ab variant was added to the assay plate and incubated at 4°C for 2 h. The wells were washed with LCIS, then fluorescein isothiocyanate (FITC)-conjugated goat anti-human IgG secondary Ab (15 μg mL^{-1}, Jackson ImmunoResearch) was added to the wells and incubated at 4°C for 1 h. The secondary Ab was removed, then 50 μL of DRAQ5 nuclear stain (1 μM prepared in LCIS; Cell Signaling, Danvers, MA, USA) was added to wells and incubated for 10 min at 4°C. The wells were washed again with LCIS and the assay plate was read using the following settings: (i) laser settings, 488 and 640 enabled, 6.0 mW; (ii) channel settings, FL-2 (488–540 nm), voltage 500 V, sensitivity 4, "Tiff files saved" and FL-4 (650–690 nm), voltage 550 V, sensitivity 4, trigger 4, "Tiff files saved"; (iii) object characteristics, FL-2 and FL-4 (peak intensity, mean intensity, median intensity and baseline); (iv) population definition, objects—cell filters (FL-4 perimeter range 20–1000 nm and FL-2 peak intensity range 0–8000 mean fluorescence intensity); and (v) population statistics, number of objects, mean (FL-2 mean intensities), median (FL-2 mean intensities), mean (FL-4 mean intensities) and median (FL-4, mean intensities). Data were analyzed using Cellista software (TTP Labtech) and GraphPad Prism 6 software. Curves were fit to the data using a one-site-specific binding with Hill slope model.

Microscale thermophoresis

MST was used to investigate the interaction between each Ab and FcγRIIIa using a Monolith NT.115 series instrument (NanoTemper Technologies, München, Germany). The extracellular domain of FcγRIIIa (158F allotype; a generous gift from Dr Shantha Raju, Janssen) was fluorescently labeled with Alexa Fluor® 647 by amine coupling (Thermo Fisher) following the manufacturer's protocol. Each Ab (199–424 μM in PBS) was serially diluted in MST buffer [50 mM Tris–HCl, pH 7.4, containing 150 mM NaCl, 10 mM $MgCl_2$, and 0.05% (v/v) Tween-20]. Labeled FcγRIIIa was then diluted in MST buffer to 42.8 nM and mixed 1:1 with each concentration of unlabeled Ab. Samples were incubated for 5 min, loaded into standard glass capillaries, and data were collected using 20% LED power and 40% MST power with the laser on for 30 s. Interactions were measured in triplicate and analyzed using the thermophoresis with T jump evaluation strategy in MO.Affinity Analysis software (NanoTemper Technologies). Affinity constants (K_Ds) were obtained by fitting the MST binding curve using a quadratic solution to the law of mass action for the fraction of fluorescent molecules that formed a complex.

^{51}Cr release assay

NK effector cells were isolated from overnight IL2-activated human PBMCs by magnetic negative selection according to the manufacturer's instructions (Miltenyi Biotec, San Diego, CA, USA). Briefly, IL2-activated PBMCs were treated with a biotin-labeled negative selection Ab cocktail (10 μL/10^7 PBMCs) followed by microbead addition and magnetic separation over a MACS column (Miltenyi Biotec). Flow-through NK cells were collected and characterized by flow cytometry, and were typically recovered in excess of 80% purity and with 5–15% yields from total PBMCs. Purified NK cells were resuspended in complete RPMI medium. MDA-MB-468 target cells were harvested by trypsinization and the pellet was directly labeled with 100 μCi of ^{51}Cr (sodium chromate in 0.9% saline; Perkin-Elmer, Waltham, MA, USA) at 37°C for 90 min with periodic mixing. Labeled target cells were washed twice with PBS and resuspended in complete RPMI medium. The ADCC assay was performed in 96-well U-bottom plates (BD Biosciences, San Jose, CA, USA) by adding titrated amounts of cetuximab or chimeric HCAb test variants at a 10:1 ratio of effector to target cells (200 μL final volume). The plates were centrifuged at 100 ×*g* for 3 min and incubated for 3–4.5 h at 37°C under a humidified atmosphere containing 5% CO_2. At the end of the assay, PBS (50 μL) was added to all wells and the cells were pelleted. Supernatant (50 μL) was removed and mixed with scintillation cocktail (150 μL, Optiphase; Perkin-Elmer) in 96-well Flex plates (Perkin-Elmer) and ^{51}Cr activity was measured using a Microbeta Trilux scintillation counter (Perkin-Elmer). The % specific lysis was calculated according to the following formula: % specific lysis = (experimental release − spontaneous release)/(maximum release − spontaneous release), where spontaneous release represents signals from tumor cells alone and maximum release represents signals from tumor cells treated with 1% (w/v) cetrimide (Sigma-Aldrich). Background cytotoxicity of IL2-activated NK cells in the absence of Ab was subtracted in the final analysis. Data were analyzed using GraphPad Prism Pro (version 6.04) and displayed as the means ± s.e.m. of triplicate measurements unless stated otherwise.

ADCC reporter assay

ADCC of cetuximab and chimeric HCAbs was measured using a reporter assay (ADCC Reporter Bioassay, V Variant; Promega, Madison, WI, USA) according to the manufacturer's instructions.[20] Briefly, freshly harvested EGFR-positive MDA-MB-468 cells (5000 cells per well in complete RPMI) were plated in wells of white 384-well flat-bottom plates (Thermo-

Fisher) along with titrated cetuximab or chimeric HCAbs. After 15 min, log-phase Jurkat reporter cells stably expressing the high-affinity FcγRIIIa receptor (25 000 cells per well; 5:1 ratio of effector to target cells) were added in complete RPMI. The plates were centrifuged at 300 $\times g$ for 3 min, and then incubated at 37°C under a humidifed atmosphere containing 5% CO_2 for 18 h. The plates were developed by adding 20 μL per well of freshly prepared luciferin reagent (BioGlo; Promega). After 10 min, luminescence was measured using a multimode microplate reader (Tecan Infinite 200 Pro, Baldwin Park, CA, USA). Data were analyzed using GraphPad Prism.

Flow cytometry

Flow cytometry was used to assess NK cell purity and to determine donor FcγRIIIa (CD16a) allotype using a multi-laser equipped LSRFortessa instrument (BD Biosciences) running FACSDiva software version 6.1.3. Briefly, ~1×10^6 PBMCs or purified NK cells were suspended in PBS containing 1% (w/v) bovine serum albumin and 0.5% (w/v) sodium azide. Labeled Abs (anti-CD3-Alexa Fluor® 405, clone UCHT-1; anti-CD45-V450, clone HI30; anti-CD56-PE, clone B159; anti-FcγRIIIa-FITC, clones 3G8 and MEM-154) were added in a volume of 100 μL and incubated at 4°C for 30 min. The cells were washed and resuspended in staining buffer containing 0.2% (w/v) propidium iodide for dead cell discrimination followed by flow analysis. FcγRIIIa allotyping was performed using a comparative analysis of cells stained with the V158-specific Ab MEM-154 and the allotype nonspecific Ab 3G8 according to a published method.[33] All labeled Abs were from BD Biosciences except for the anti-CD3 Ab, clone UCHT-1 (Bio-Rad). Data were analyzed using FlowJo software (version 7.6.5; BD Biosciences).

ACKNOWLEDGMENTS

We gratefully acknowledge Qingling Yang for excellent technical assistance. We thank Roger MacKenzie for help in interpreting surface plasmon resonance experiments.

CONFLICT OF INTEREST

The authors have no conflicts of interest to declare.

REFERENCES

1. Scott AM, Wolchok JD, Old LJ. Antibody therapy of cancer. *Nat Rev Cancer* 2012; **12**: 278–287.
2. Weng WK, Levy R. Two immunoglobulin G fragment C receptor polymorphisms independently predict response to rituximab in patients with follicular lymphoma. *J Clin Oncol* 2003; **21**: 3940–3947.
3. Zhang W, Gordon M, Schultheis AM, *et al.* FCGR2A and FCGR3A polymorphisms associated with clinical outcome of epidermal growth factor receptor expressing metastatic colorectal cancer patients treated with single-agent cetuximab. *J Clin Oncol* 2007; **25**: 3712–3718.
4. Musolino A, Naldi N, Bortesi B, *et al.* Immunoglobulin G fragment C receptor polymorphisms and clinical efficacy of trastuzumab-based therapy in patients with HER-2/neu-positive metastatic breast cancer. *J Clin Oncol* 2008; **26**: 1789–1796.
5. van Sorge NM, van der Pol WL, van de Winkel JG. FcγR polymorphisms: implications for function, disease susceptibility and immunotherapy. *Tissue Antigens* 2003; **61**: 189–202.
6. Park HI, Yoon HW, Jung ST. The highly evolvable antibody Fc domain. *Trends Biotechnol* 2016; **34**: 895–908.
7. Ferrara C, Grau S, Jager C, *et al.* Unique carbohydrate-carbohydrate interactions are required for high affinity binding between FcγRIII and antibodies lacking core fucose. *Proc Natl Acad Sci U S A* 2011; **108**: 12669–12674.
8. Junttila TT, Parsons K, Olsson C, *et al.* Superior *in vivo* efficacy of afucosylated trastuzumab in the treatment of HER2-amplified breast cancer. *Cancer Res* 2010; **70**: 4481–4489.
9. Michaelsen TE, Aase A, Norderhaug L, Sandlie I. Antibody dependent cell-mediated cytotoxicity induced by chimeric mouse-human IgG subclasses and IgG3 antibodies with altered hinge region. *Mol Immunol* 1992; **29**: 319–326.
10. Redpath S, Michaelsen TE, Sandlie I, Clark MR. The influence of the hinge region length in binding of human IgG to human Fcγ receptors. *Hum Immunol* 1998; **59**: 720–727.
11. Giuntini S, Granoff DM, Beernink PT, Ihle O, Bratlie D, Michaelsen TE. Human IgG1, IgG3, and IgG3 hinge-truncated mutants show different protection capabilities against meningococci depending on the target antigen and epitope specificity. *Clin Vaccine Immunol* 2016; **23**: 698–706.
12. Brekke OH, Michaelsen TE, Sandin R, Sandlie I. Activation of complement by an IgG molecule without a genetic hinge. *Nature* 1993; **363**: 628–630.
13. Gillies SD, Wesolowski JS. Antigen binding and biological activities of engineered mutant chimeric antibodies with human tumor specificities. *Hum Antibodies Hybridomas* 1990; **1**: 47–54.
14. Dall'Acqua WF, Cook KE, Damschroder MM, Woods RM, Wu H. Modulation of the effector functions of a human IgG1 through engineering of its hinge region. *J Immunol* 2006; **177**: 1129–1138.
15. Yan B, Boyd D, Kaschak T, *et al.* Engineering upper hinge improves stability and effector function of a human IgG1. *J Biol Chem* 2012; **287**: 5891–5897.
16. Hamers-Casterman C, Atarhouch T, Muyldermans S, *et al.* Naturally occurring antibodies devoid of light chains. *Nature* 1993; **363**: 446–448.
17. Bell A, Wang ZJ, Arbabi-Ghahroudi M, *et al.* Differential tumor-targeting abilities of three single-domain antibody formats. *Cancer Lett* 2010; **289**: 81–90.
18. Rossotti MA, Henry KA, van Faassen H, *et al.* Camelid single-domain antibodies raised by DNA immunization are potent inhibitors of EGFR signaling. *Biochem J* 2018; **476**: 39–50.

19. Li P, Jiang N, Nagarajan S, Wohlhueter R, Selvaraj P, Zhu C. Affinity and kinetic analysis of Fcγ receptor IIIa (CD16a) binding to IgG ligands. *J Biol Chem* 2007; **282**: 6210–6221.
20. Cheng ZJ, Garvin D, Paguio A, *et al.* Development of a robust reporter-based ADCC assay with frozen, thaw-and-use cells to measure Fc effector function of therapeutic antibodies. *J Immunol Methods* 2014; **414**: 69–81.
21. Liu B, Spearman M, Doering J, Lattova E, Perreault H, Butler M. The availability of glucose to CHO cells affects the intracellular lipid-linked oligosaccharide distribution, site occupancy and the *N*-glycosylation profile of a monoclonal antibody. *J Biotechnol* 2014; **170**: 17–27.
22. Radaev S, Motyka S, Fridman WH, Sautes-Fridman C, Sun PD. The structure of a human type III Fcγ receptor in complex with Fc. *J Biol Chem* 2001; **276**: 16469–16477.
23. Bakalar MH, Joffe AM, Schmid EM, Son S, Podolski M, Fletcher DA. Size-dependent segregation controls macrophage phagocytosis of antibody-opsonized targets. *Cell* 2018; **174**: 131–142. e113.
24. Cleary KLS, Chan HTC, James S, Glennie MJ, Cragg MS. Antibody distance from the cell membrane regulates antibody effector mechanisms. *J Immunol* 2017; **198**: 3999–4011.
25. Henry KA, MacKenzie CR. Antigen recognition by single-domain antibodies: structural latitudes and constraints. *MAbs* 2018; **10**: 815–826.
26. Brooks CL, Rossotti MA, Henry KA. Immunological functions and evolutionary emergence of heavy-chain antibodies. *Trends Immunol* 2018; **39**: 956–960.
27. Zhang J, Liu X, Bell A, *et al.* Transient expression and purification of chimeric heavy chain antibodies. *Protein Expr Purif* 2009; **65**: 77–82.
28. Tayi VS, Butler M. Isolation and quantification of *N*-glycans from immunoglobulin G antibodies for quantitative glycosylation analysis. *J Biol Methods* 2015; **2**: e19.
29. Guile GR, Rudd PM, Wing DR, Prime SB, Dwek RA. A rapid high-resolution high-performance liquid chromatographic method for separating glycan mixtures and analyzing oligosaccharide profiles. *Anal Biochem* 1996; **240**: 210–226.
30. Hussack G, Hirama T, Ding W, Mackenzie R, Tanha J. Engineered single-domain antibodies with high protease resistance and thermal stability. *PLoS ONE* 2011; **6**: e28218.
31. Patel TR, Nikodemus D, Besong TMD, *et al.* Biophysical analysis of a lethal laminin α-1 mutation reveals altered self-interaction. *Matrix Biol* 2016; **49**: 93–105.
32. Krahn N, Meier M, To V, *et al.* Nanoscale assembly of high-mobility group AT-hook 2 protein with DNA replication fork. *Biophys J* 2017; **113**: 2609–2620.
33. Meier M, Moya-Torres A, Krahn NJ, *et al.* Structure and hydrodynamics of a DNA G-quadruplex with a cytosine bulge. *Nucleic Acids Res* 2018; **46**: 5319–5331.
34. Dam J, Schuck P. Calculating sedimentation coefficient distributions by direct modeling of sedimentation velocity concentration profiles. *Methods Enzymol* 2004; **384**: 185–212.
35. Schuck P. Sedimentation analysis of noninteracting and self-associating solutes using numerical solutions to the Lamm equation. *Biophys J* 1998; **75**: 1503–1512.
36. Laue TM, Shah BD, Ridgeway TM, Pelletier SL. Computer-aided interpretation of analytical sedimentation data for proteins. In: Harding SE, Rowe AJ, Horton JC, eds. Analytical Ultracentrifugation in Biochemistry and Polymer Science. Cambridge, UK: Royal Society of Chemistry; 1992: 90–125.

SUPPORTING INFORMATION

Additional supporting information may be found online in the Supporting Information section at the end of the article.

© 2019 National Research Council Canada and Australasian Society for Immunology Inc.